


Study of Flat Spectrum Radio Quasars and BL Lacertae Objects as Sources of Diffusive Ultra High-Energy Cosmic Rays

Swaraj Pratim Sarmah * and Umananda Dev Goswami [†]

*High-Energy Astrophysics and Cosmology (HEAC) Group,
Department of Physics, Dibrugarh University, Dibrugarh, 786004, Assam, India*

We examine whether Flat Spectrum Radio Quasars (FSRQs) and BL Lacertae objects (BL Lacs) can act as plausible astrophysical sources of diffuse ultra-high-energy cosmic rays (UHECRs). Using realistic luminosity-dependent density evolution (LDDE) functions derived from observed gamma-ray luminosity functions for FSRQs and BL Lacs, we calculate the redshift evolution of the cosmic ray source population through integrated luminosity functions. The diffuse UHECRs flux from these sources is modelled by propagating nuclei through extragalactic space, including energy losses from interactions with cosmic photon backgrounds. The resulting UHECRs spectra are compared with observational data from the Pierre Auger Observatory and the Telescope Array, with fluxes normalised at reference energies. In addition to spectral comparisons, we generate HEALPix-based sky maps and identify potential hotspots. Near these hotspots, several galaxies and extragalactic sources are found, suggesting possible associations with the enhanced flux regions. Our results indicate that LDDE-modelled AGNs could contribute significantly to the observed diffuse UHECRs flux and provide constraints on their role as dominant sources.

I. INTRODUCTION

The origin of ultra high-energy cosmic rays (UHECRs; $E \gtrsim 10^{17}$ eV) remains as one of the outstanding puzzles in modern astrophysics (for reviews, see [1, 2]). Unlike photons and neutrinos, the arrival directions of UHECRs are obscured due to deflections in galactic and extragalactic magnetic fields [3, 4], complicating the task of identifying their sources. Although the observed features in the UHECRs spectrum suggest an extragalactic origin, the precise energy at which the transition between galactic and extragalactic contributions occurs is still uncertain (e.g., see [5]). The Pierre Auger Observatory (Auger) in Argentina [6] and the Telescope Array (TA) in Utah, USA [7], currently provide the most detailed measurements of these particles.

A few spectacular events recorded in different UHECR experiments already highlight the involvement of extreme energies in such events. E.g., the “Oh-My-God” particle, detected by the Fly’s Eye experiment, carried an estimated energy of ≈ 320 EeV ($1 \text{ EeV} = 10^{18}$ eV), making it the most energetic event recorded via the fluorescence technique [8]. More recently, the TA Collaboration reported the “Amaterasu” event on May 27, 2021, which is the most energetic cosmic ray (CR) ever detected with a surface detector array. Its reconstructed energy of 244 ± 29 (stat) $_{-76}^{+51}$ (sys) EeV and arrival direction (RA, Dec) of $(255.9^\circ \pm 0.6^\circ, 16.1^\circ \pm 0.5^\circ)$ places it among the most energetic particles observed to date [9]. Such extreme-energy events raise the fundamental question about their acceleration mechanisms and astrophysical origins.

Propagation effects, i.e., the effects of the environ-

mental situations on CRs while they propagate through space, also play a crucial role in their properties, including flux, energy and arrival directions from their sources. At the highest energies, UHECRs are expected to suffer significant attenuation due to the Greisen–Zatsepin–Kuz’min (GZK) suppression [10, 11], arising from photopion production with the cosmic microwave background (CMB) photons. The attenuation length of protons at these energies is of order ~ 10 Mpc (e.g., see [12]). Composition studies add further complexity: while TA results suggest predominantly light primaries at $E \gtrsim 10^{19}$ eV, significant uncertainties still remain [13].

Several astrophysical and cosmological scenarios have been proposed to account for the sources of UHECRs, which include ultraheavy nuclei [14], binary neutron star mergers [15], the decay of superheavy dark matter [16], and transient events in unresolved galaxies [17]. In addition, cosmological scenarios based on modified or alternative gravity theories provide an alternative framework to explain the acceleration, propagation, and large-scale distribution of UHECRs in the evolving Universe [18, 19]. Moreover, UHECRs are powerful probes of new physics such as Lorentz invariance violation (LIV) [20], and this possibility has also been explored for the Amaterasu event [21]. Recent high-precision measurements of UHECRs reveal several characteristic features: a hardening near the ankle at ~ 5 EeV [22–24], a subsequent steepening at ~ 13 EeV [23, 25], and a strong suppression beyond ~ 50 EeV [26, 27]. Composition studies based on the depth of shower maximum, X_{max} , show that UHECRs are relatively light at a few EeV and become progressively heavier with increasing energy. Moreover, the narrow dispersion in X_{max} above the ankle suggests that the mass distribution at a given energy is relatively tight.

When these observations are interpreted within astrophysical source models, they indicate that two distinct source populations are required to explain the UHECRs

* swarajpratimsarmah16@gmail.com

† umananda@dibru.ac.in

flux above ~ 1 EeV and across the ankle [28–30]. The low-energy (LE) population, dominant below a few EeV, is likely composed of light and intermediate nuclei (H, He, N) with steep spectra $\propto E^{-\gamma_L}$, where $\gamma_L \simeq 3 - 3.7$, and with an only loosely constrained rigidity cutoff. At higher energies, the high-energy (HE) population becomes dominant, consisting of progressively heavier nuclei. This component is expected to have a much harder injection spectrum $\propto E^{-\gamma_H}$, with $\gamma_H < 1$, and in some scenarios even negative spectral indices. Together, these populations provide a consistent description of the observed UHECRs spectrum and composition, linking spectral features to the physics of acceleration and propagation.

The study of radio-loud (RL) active galactic nuclei (AGN), particularly blazars with strongly relativistic and beamed jets, provides a unique method to probe jet activity, black hole spin, and the role of major mergers in galaxy evolution. A key statistical tool in this context is the luminosity function (LF) of blazars, defined as the number of blazars per comoving volume within a given luminosity interval, and its evolution with redshift. The Fermi Gamma-ray Space Telescope (*Fermi-LAT*) has revolutionized this field: thanks to its sensitivity and all-sky uniform coverage, it has detected hundreds of blazars spanning from the local Universe up to $z = 3.1$ [31]. The blazar LF not only constrains their contribution to the diffuse extragalactic γ -ray background but also helps establish connections between blazars and their parent AGN populations [32, 33]. Extensive multiwavelength studies of blazars have been carried out in the radio [34, 35] and soft X-ray [36–41] bands. Flat-spectrum radio quasars (FSRQs), the most luminous subclass of blazars, exhibit strong positive cosmological evolution, meaning they were more numerous in the past [34]. This trend persists up to a luminosity-dependent redshift cutoff (e.g., see [41, 42]). Interestingly, FSRQs follow an evolutionary pattern similar to that of X-ray-selected, radio-quiet AGNs [43–45], suggesting possible common mechanisms driving their cosmic evolution.

Another important sub-population of blazars are BL Lacertae (BL Lac) objects (e.g., see [46]). They represent an extreme class of AGNs characterized by highly variable emission, most likely produced by relativistic jets aligned very close to our line of sight. BL Lac objects are distinguished from their FSRQ counterparts by their optical spectra, which lack significant emission lines with equivalent width $> 5\text{\AA}$ (e.g., see [47, 48]). Their spectra are typically dominated by a power-law continuum, indicating either exceptionally strong non-thermal jet emission (aligned nearly directly with our line of sight), or unusually weak thermal disk and broad-line emission, the latter plausibly linked to low accretion activity [49].

Considering the said interesting nature of emission with high redshift values of FSRQs and BL Lac objects, we aim to investigate these objects as plausible sources of UHECRs from the perspective of the characteristics of UHE fluxes from them. Thus, the remainder of the paper is organised as follows. Section II is divided into two sub-

sections. In Subsection II A, we describe the evolution of FSRQ sources, while Subsection II B focuses on the evolution of BL Lac objects. Section III presents the basic equations governing the propagation of UHECRs. In Section IV, we provide the flux calculation equations, discuss the corresponding mixed composition results, generate skymaps, identify hotspots, and locate nearby galaxies within 1° angular separation. Finally, Section V summarises the findings and draws conclusions of the study.

II. EVOLUTION OF AGN SOURCES

In this section, we describe the evolution of two classes of AGN sources, viz., the FSRQs and BL Lac objects, which we consider as potential sources of UHECRs, as mentioned already. First, we describe the FSRQs’ evolution, and in the next the evolution of the BL Lac objects is discussed as follows.

A. Flat Spectrum Radio Quasars (FSRQs)

The space density of radio-quiet AGNs is observed to reach a maximum at intermediate redshifts. The epoch of this ‘redshift peak’ is correlated with the luminosity of the sources (e.g., see [43, 44]). This peak likely reflects the combined effects of supermassive black hole (SMBH) growth over cosmic time and a decline in fuelling activity as the frequency of major mergers decreases at later times. To investigate whether similar behaviour occurs in the *Fermi-LAT* FSRQ population, Ajello et al. fit the data using a pure luminosity evolution (PLE) model as described in Ref. [50] and is given as

$$\Phi(L_\gamma, z) = \Phi(L_\gamma/e(z)), \quad (1)$$

where

$$\begin{aligned} \Phi(L_\gamma/e(z=0)) &= \frac{dN}{dL_\gamma} = \frac{A}{2.303 L_\gamma} \\ &\times \left[\left(\frac{L_\gamma}{L_*} \right)^{\gamma_1} + \left(\frac{L_\gamma}{L_*} \right)^{\gamma_2} \right]^{-1} \end{aligned} \quad (2)$$

and

$$e(z) = (1+z)^k e^{z/\xi}. \quad (3)$$

In the PLE model, the comoving luminosity function $\Phi(L_\gamma, z)$ is assumed to evolve only in luminosity, such that the redshift dependence enters through the evolution factor $e(z)$. Here, L_γ denotes the γ -ray luminosity of the source and $\Phi(L_\gamma, z)$ gives the number density of sources per unit luminosity. The local luminosity function at $z = 0$ is characterized by a broken power-law with a normalization factor A , break luminosity L_* , low-luminosity slope γ_1 , and high-luminosity slope γ_2 , where γ_1 controls the behavior of the faint-end population ($L_\gamma \ll L_*$) and

γ_2 determines the fall-off at the bright end ($L_\gamma \gg L_*$). The luminosity evolution factor, $e(z) = (1+z)^k \exp(z/\xi)$, describes how the characteristic luminosity shifts with redshift, where k sets the strength of luminosity evolution and ξ controls the redshift scale at which the evolution transits or saturates. As a simple PLE function model does not adequately reproduce the *Fermi-LAT* data, and given evidence for a luminosity-dependent evolution of the redshift peak, we fit the *Fermi-LAT* FSRQ sample using a luminosity-dependent density evolution (LDDE) model. In this approach, the evolution occurs mainly in density, with the redshift peak depending on luminosity. The LDDE model is parametrised as in Ref. [50], which is

$$\Phi(L_\gamma, z) = \Phi(L_\gamma) \times e(z, L_\gamma), \quad (4)$$

where

$$e(z, L_\gamma) = \left[\left(\frac{1+z}{1+z_c(L_\gamma)} \right)^{p_1} + \left(\frac{1+z}{1+z_c(L_\gamma)} \right)^{p_2} \right]^{-1} \quad (5)$$

and

$$z_c(L_\gamma) = z_c^* \cdot (L_\gamma/10^{48})^\alpha. \quad (6)$$

Here, $z_c(L_\gamma)$ represents the luminosity-dependent redshift at which the evolutionary trend changes sign (from positive to negative), with z_c^* denoting the redshift peak for an FSRQ of luminosity $10^{48} \text{ erg s}^{-1}$ and the parameter α controls how the peak redshift shifts with luminosity. The evolution factor $e(z, L_\gamma)$ is parametrized by two evolutionary indices, p_1 and p_2 , which describe the redshift evolution below and above the luminosity-dependent peak redshift $z_c(L_\gamma)$, respectively. The values of all parameters are adopted from Ref. [50]. $\Phi(L_\gamma)$ adopts the same double power-law form as in Eq. (2). This parametrisation is similar to that proposed by Ref. [43], but it is continuous around the redshift peak $z_c(L_\gamma)$. Such continuity is advantageous for fitting algorithms that use derivatives of the function to locate the minimum.

B. BL Lacertae (BL Lac) Objects

In this case, we use the intrinsic distribution of photon indices following Ref. [51], where the photon index Γ is assumed to follow a Gaussian distribution for a given redshift z and luminosity L_γ and hence the luminosity function becomes

$$\Phi(L_\gamma, z, \Gamma) \propto \exp \left[-\frac{(\Gamma - \mu(L_\gamma))^2}{2\sigma^2} \right], \quad (7)$$

where μ and σ are the Gaussian mean and dispersion, respectively. Previous works [52, 53] have suggested that the mean photon index may correlate with luminosity, and thus we allow μ to vary with L_γ following the blazar sequence prescription of Ref. [51], given by

$$\mu(L_\gamma) = \mu^* + \beta [\log_{10}(L_\gamma) - 46], \quad (8)$$

where μ^* is the mean photon index at a reference luminosity $L_\gamma = 10^{46} \text{ erg s}^{-1}$, and β quantifies the slope of the luminosity–spectral index correlation. The LF at redshift $z = 0$ is modelled as a smoothly connected double power law, multiplied by the photon index distribution, given in Eq. (7), as

$$\Phi(L_\gamma, z = 0, \Gamma) = \frac{A}{2.303 L_\gamma} \left[\left(\frac{L_\gamma}{L_*} \right)^{\gamma_1} + \left(\frac{L_\gamma}{L_*} \right)^{\gamma_2} \right]^{-1} \exp \left[-\frac{(\Gamma - \mu(L_\gamma))^2}{2\sigma^2} \right] \quad (9)$$

Here also, we utilise the same formalism as performed in Eqs. (4)–(6) and the best fit values of the parameters are adopted from Ref. [51].

III. DIFFUSION OF COSMIC RAYS IN TURBULENT MAGNETIC FIELDS

Modelling extragalactic magnetic fields remains a complex task due to several uncertainties and limitations [54]. The exact strength and structure of these fields are still not well known and can vary greatly across different parts of extragalactic space [55, 56]. To make the study more manageable, we consider the propagation of CRs in a uniform and turbulent extragalactic magnetic field. Such a field is described by two key parameters: its root mean square (RMS) strength B and its coherence length l_c . The RMS strength, defined as $\sqrt{\langle B^2(x) \rangle}$, may be as weak as 10^{-16} G in cosmic voids [57], increase up to $\gtrsim 10 \text{ nG}$ in galaxy clusters, and typically reach about 1 nG in filaments [58–60]. The coherence length l_c generally lies between 0.01 Mpc and 1 Mpc [3]. The effective Larmor radius r_L of a charged particle with charge Ze and energy E moving through a turbulent magnetic field of strength B can then be written as

$$r_L = \frac{E}{ZeB} \simeq 1.1 \frac{E/\text{EeV}}{ZB/\text{nG}} \text{ Mpc}. \quad (10)$$

The idea of critical energy is essential for describing how charged particles diffuse in magnetic fields. It is the energy at which the coherence length of a particle with charge Ze becomes equal to its Larmor radius, i.e., $r_L(E_c) = l_c$. Hence, the critical energy is written as

$$E_c = ZeBl_c \simeq 0.9Z \frac{B}{\text{nG}} \frac{l_c}{\text{Mpc}} \text{ EeV}. \quad (11)$$

This energy separates two different diffusion regimes: resonant diffusion at energies below E_c and non-resonant diffusion at energies above E_c .

The energy-dependent diffusion coefficient D is expressed as [61]

$$D(E) \simeq \frac{cl_c}{3} \left[4 \left(\frac{E}{E_c} \right)^2 + a_1 \left(\frac{E}{E_c} \right) + a_L \left(\frac{E}{E_c} \right)^{2-\gamma} \right], \quad (12)$$

where γ is the spectral index, and a_I and a_L are constants. For a Kolmogorov-type turbulence spectrum, $\gamma = 5/3$ with $a_L \approx 0.23$ and $a_I \approx 0.9$. As noted earlier, the diffusion length l_D represents the typical distance over which a particle's total deflection becomes roughly one radian, defined as $l_D = 3D/c$.

In the diffusive regime, the transport equation for UHE particles moving through an expanding Universe from a source at position x_s is given by [62]

$$\begin{aligned} \frac{\partial n}{\partial t} + 3H(t)n - b(E, t) \frac{\partial n}{\partial E} - n \frac{\partial n}{\partial E} - \frac{D(E, t)}{a^2(t)} \nabla^2 n \\ = \frac{\mathcal{N}(E, t)}{a^3(t)} \delta^3(x - x_s), \end{aligned} \quad (13)$$

where the Hubble parameter is $H(t) = \dot{a}(t)/a(t)$, with $\dot{a}(t)$ representing the rate of change of the scale factor $a(t)$ over cosmic time t . The coordinates x denote comoving positions, n is the particle density, and $\mathcal{N}(E)$ represents the source emissivity. At a time t corresponding to redshift z , the separation between the source and the particle is given by $r_s = x - x_s$. Energy losses caused by the expansion of the Universe and interactions with the CMB are included in this formulation as

$$\frac{dE}{dt} = -b(E, t), \quad b(E, t) = H(t)E + b_{\text{int}}(E). \quad (14)$$

Here, $H(t)E$ corresponds to adiabatic energy losses due to the expansion of the Universe, while $b_{\text{int}}(E)$ represents energy losses arising from interactions. UHECRs may interact with both the CMB and extragalactic background light (EBL). In this study, however, we consider only the energy losses caused by interactions with the CMB, which include processes such as pair production and photopion production [61].

The general solution to Eq. (13) was derived in Ref. [62] and is written as

$$n(E, r_s) = \int_0^{z_i} dz \left| \frac{dt}{dz} \right| \mathcal{N}(E_g, z) \frac{\exp[-r_s^2/4\lambda^2]}{(4\pi\lambda^2)^{3/2}} \frac{dE_g}{dE}, \quad (15)$$

where λ is the Syrovatskii variable, defined as [63]

$$\lambda^2(E, z) = \int_0^z dz \left| \frac{dt}{dz} \right| (1+z)^2 D(E_g, z). \quad (16)$$

Here, $E_g(E, z)$ is the generation energy at redshift z corresponding to an observed energy E at $z = 0$. The relation between cosmological time and redshift for standard Λ CDM model is given by

$$\left| \frac{dt}{dz} \right| = \frac{1}{H_0(1+z)\sqrt{(1+z)^3\Omega_m + \Omega_\Lambda}}, \quad (17)$$

where, $H_0 = 67.4 \text{ km s}^{-1} \text{ Mpc}^{-1}$, $\Omega_m = 0.315$, and $\Omega_\Lambda = 0.699$ according to the Planck's data [64]. In the diffusive regime, the particle density depends on the particle energy, the distance from the source, and the properties of the turbulent magnetic field (TMF). Diffusion can

cause the observed density of CRs at a given distance to be considerably higher than what would be expected for rectilinear propagation, which follows a $1/r^2$ law. This enhancement results from delayed escape and multiple scattering of particles, and is quantified by the enhancement factor, defined as the ratio of the diffusive density to the rectilinear density [65] as given by

$$\xi(E, r_s) = \frac{4\pi r_s^2 c n(E, r_s)}{\mathcal{N}(E)}. \quad (18)$$

IV. FLUX OF UHECRS

The diffusion of CRs in TMFs has been studied extensively by many authors [3, 62, 66–78]. Berezhinsky and Gazizov [62, 79] generalised the Syrovatskii solution [63] to examine the diffusion of protons in an expanding Universe. The flux from a CR source at a distance r_s , much larger than the diffusion length l_D , can be obtained by solving the diffusion equation in an expanding Universe [62], leading to the expression [80]:

$$J(E) = \frac{c}{4\pi} \int_0^{z_{\text{max}}} dz \left| \frac{dt}{dz} \right| \mathcal{N}[E_g(E, z), z] \frac{\exp[-r_s^2/(4\lambda^2)]}{(4\pi\lambda^2)^{3/2}} \frac{dE_g}{dE}, \quad (19)$$

where z_{max} is the maximum redshift at which the source starts emitting CRs, and E_g is the generation energy at redshift z corresponding to energy E at $z = 0$.

The total source emissivity \mathcal{N} is obtained by summing the charge-specific emissivities \mathcal{N}_Z for different nuclei. The charge-specific emissivity follows a power-law with a rigidity cutoff ZE_{max} and is given by [81]

$$\mathcal{N}_Z(E, z) = \varepsilon_Z f(z) E^{-\gamma} / \cosh(E/ZE_{\text{max}}), \quad (20)$$

where ε_Z denotes the relative contribution of nuclei with charge Z to the CR flux, and $f(z)$ describes the evolution of source emissivity with redshift z . In our study, we improve the description of $f(z)$ by adopting the luminosity-dependent density evolution (LDDE) model for FSRQs derived by Ajello et al. [50]. Instead of using a simple phenomenological form, often taken as a power-law or broken power-law in $(1+z)$, we employ a physically motivated redshift evolution based on the observed FSRQ luminosity function. In this framework, the comoving source density is expressed as

$$f(z) = E^{-\gamma} \int_{L_{\text{min}}}^{L_{\text{max}}} \Phi(L, z) L dL, \quad (21)$$

where $\Phi(L, z)$ is the luminosity function of the sources and L_{min} , L_{max} are the luminosity limits. This integration properly incorporates the redshift and luminosity dependence of the AGN population. This approach ensures that the source evolution is not arbitrary, but directly informed by observational data, providing a more realistic

representation of UHECR source emissivity. In contrast, simple phenomenological forms such as $f(z) \propto (1+z)^m$ or broken power-laws do not account for the luminosity dependence of AGNs and may result in oversimplified or biased estimates of source evolution. The Ajello LDDE model thus offers a robust, observation-based framework for modelling UHECR source evolution.

Equation (19) can be generalised to nuclei in terms of their rigidity. During photo-disintegration, the rigidity and Lorentz factor of the primary fragment are largely conserved, minimally affecting the diffusion of the particle. However, these processes introduce complications because the source term \mathcal{N} refers to the primary nucleus responsible for the observed fragment, and establishing this connection is challenging due to the stochastic nature of disintegration. This issue was discussed in Ref. [81], and we extend this discussion within modified and alternative gravity frameworks [82, 83].

For multiple sources, we apply the propagation theorem [84] to sum contributions from all sources, which satisfies

$$\int_0^\infty dr, 4\pi r^2 \frac{\exp[-r^2/(4\lambda^2)]}{(4\pi\lambda^2)^{3/2}} = 1. \quad (22)$$

To examine the effect of finite source distances on flux suppression, we compute the sum over a given set of distance distributions. These assume a uniform source density, with distances from the observer given by [80, 81, 85]

$$r_i = \left(\frac{3}{4\pi}\right)^{1/3} d_s \frac{\Gamma(i+1/3)}{(i-1)!}, \quad (23)$$

where d_s is the separation distance between sources. For a discrete source distribution, summing over all sources yields a suppression factor [80, 81]

$$F \equiv \frac{1}{n_s} \sum_i \frac{\exp[-r_i^2/4\lambda^2]}{(4\pi\lambda^2)^{3/2}}, \quad (24)$$

in place of Eq. (22), where n_s is the source density. Using Eq. (19), after summing over all sources, the modified flux for an ensemble of sources can then be expressed as

$$J_{\text{mod}}(E) \simeq \frac{R_H n_s}{4\pi} \int_0^{z_{\text{max}}} dz (1+z)^{-1} \left| \frac{dt}{dz} \right| \times \mathcal{N}[E_g(E, z), z] \frac{dE_g}{dE} F, \quad (25)$$

where $R_H = c/H_0 = 4.3$ Gpc is known as the Hubble radius. We can rewrite Eq. (16) in terms of R_H and from Eq. (12) as

$$\lambda^2(E, z) = \frac{H_0 R_H l_c}{3} \int_0^z dz \left| \frac{dt}{dz} \right| (1+z)^2 \left[4 \left(\frac{(1+z)E}{E_c} \right)^2 + a_I \left(\frac{(1+z)E}{E_c} \right) + a_L \left(\frac{(1+z)E}{E_c} \right)^{2-\gamma} \right]. \quad (26)$$

For the mixed composition case, we draw Fig. 1 for the fluxes along with the mean depths of shower maximum $\langle X_{\text{max}} \rangle$ as predicted by our theoretical calculations. The nuclear abundance of p, He, N, Si and Fe is mentioned at the top of the plots. Since we use two different AGN source population, so we get two different separation distance in fitting the numerical results with Auger and TA data. The corresponding values of the source separation distances are 160 kpc and 0.2 Mpc for FSRQs and BL Lac objects, respectively. The depth of the shower maximum, X_{max} , is determined using a parametrization based on air shower physics [86, 87]. For a nucleus with mass number A and energy E , it is expressed as [86, 87].

$$X_{\text{max}}(E, A) = X_0 + \nu \ln \left(\frac{E}{A} \right), \quad (27)$$

where X_0 and ν are parameters influenced by hadronic interactions [86]. In our analysis, we have used the values as $X_0 = 700 \text{ g cm}^{-2}$ and $\nu = 50 \text{ g cm}^{-2}$ [87, 88]. For scenarios involving a mixed composition of CRs, the flux-weighted mean depth of the shower maximum is computed as

$$\langle X_{\text{max}} \rangle = \frac{\sum_i J_i(E) \cdot X_{\text{max}, i}(E, A_i)}{\sum_i J_i(E)}. \quad (28)$$

Here, $J_i(E)$ denotes the flux of each nuclear species.

We provide the χ^2 test for both source models with Auger and TA data, and it is defined as

$$\chi^2 = \sum_i \frac{(J_{\text{th}}^i - J_{\text{obs}}^i)^2}{\sigma_i^2}, \quad (29)$$

where J_{th}^i are the theoretical values of flux obtained from our calculations and J_{obs}^i are the observed flux values, which are obtained from the Auger and the TA experiment. σ denotes the total uncertainty in each energy bin, incorporating both statistical and systematic errors. The corresponding reduced χ^2 values with the combined Auger and TA data are 2.02 and 2.43 for FSRQs and BL Lac objects respectively.

Fig. 1 also displays the fluxes for a mixed composition of nuclei along with the corresponding $\langle X_{\text{max}} \rangle$ s and $\sigma(X_{\text{max}})$ s at the redshift $z_{\text{max}} = 1$. The parametrisations show deviations from a purely proton composition, and the influence of the astrophysical source model is also apparent. The observational data for $\langle X_{\text{max}} \rangle$ s from Auger and TA are taken from Refs. [89, 90]. These datasets provide $\langle X_{\text{max}} \rangle$ values along with statistical errors and uncertainties. In the $\langle X_{\text{max}} \rangle$ and $\sigma(X_{\text{max}})$ plots, the statistical uncertainties are shown as shaded bands. The good agreement between our results and the observational data supports the validity of the source models used in reproducing the CR spectra. For readability, we include Table I, which summarizes the key parameters used in fitting the UHECR energy spectrum with the Auger and

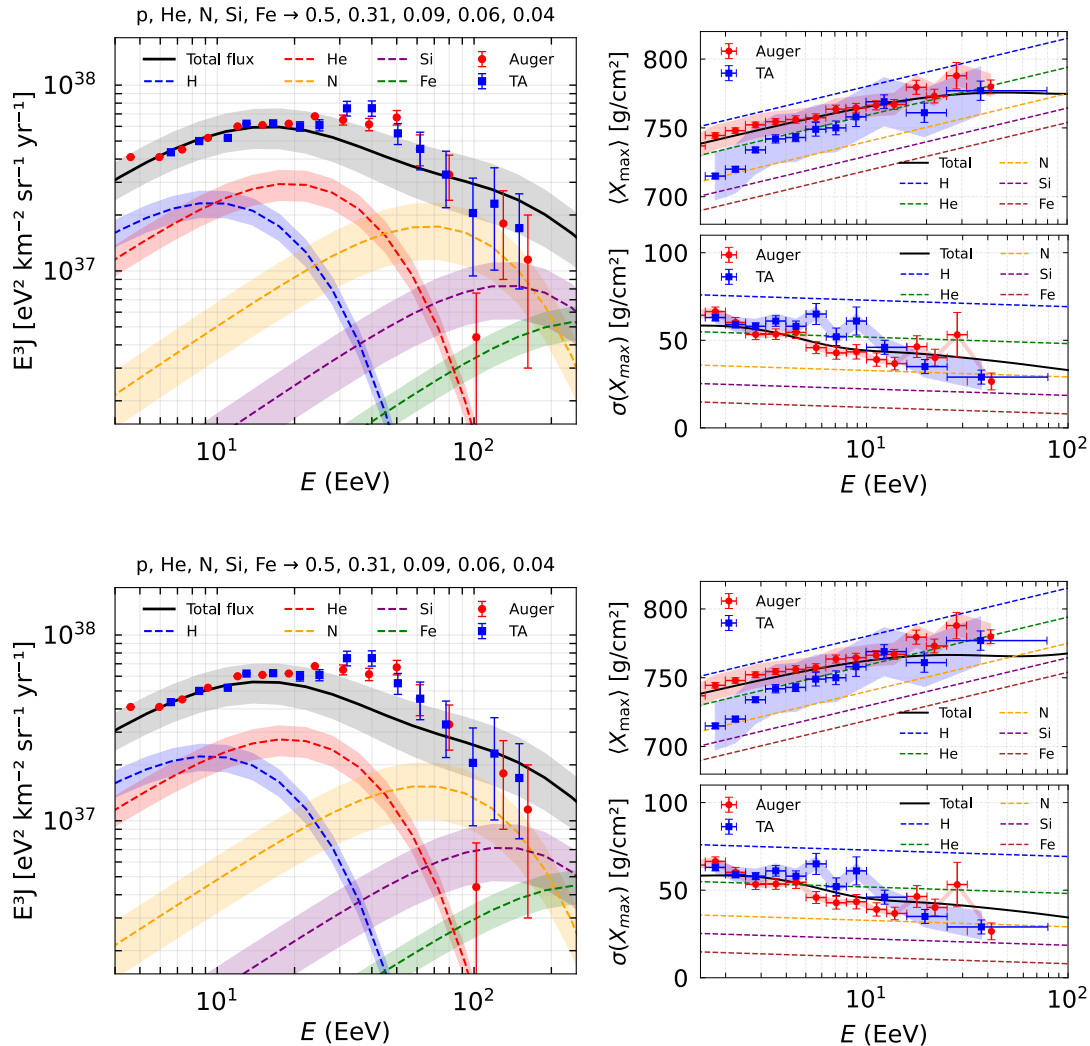


FIG. 1. Fluxes of UHECRs and X_{\max} values for a mixed composition scenario from FSRQs (top panel) and BL Lac objects (bottom panel), obtained by using different source separation distances (see text) and varying relative abundances of nuclear species. The fluxes and X_{\max} values are compared with Auger and TA measurements.

TABLE I. Comparison of parameters for FSRQs and BL Lac objects.

Parameters	FSRQ	BL Lac
d_s	160 kpc	0.2 Mpc
E_{\max} (EeV)	$5Z$	$5Z$
χ_{red}^2	2.02	2.43
d.o.f.	19	16

TA observational data for the FSRQ and BL Lac source classes.

To model the CRs flux distributions, we use the HEALPix [91] framework with a resolution of $N_{\text{side}} = 256$, corresponding to $N_{\text{pix}} = 12 \times N_{\text{side}}^2$ pixels covering the entire sky. Source positions are distributed uniformly in right ascension (RA) and declination (Dec),

where RA ranges from 0° to 360° and Dec from -90° to 90° . These coordinates are converted into HEALPix angular coordinates (θ, ϕ) using $\theta = 90^\circ - \text{Dec}$ and $\phi = \text{RA}$. The HEALPix pixel indices are obtained with `healpy.ang2pix`. To construct the flux maps, predefined flux values are assigned to each pixel, summing contributions from all sources in the pixel. A Gaussian smoothing filter with an angular scale of 2° is applied using `healpy.smoothing` to ensure spatial smoothness. The maps are normalised with a logarithmic stretch to enhance contrast, replacing zero-valued pixels with a small nonzero value to avoid numerical artefacts. For visualisation, Mollweide projections [91] with a logarithmic colour scale are used, where longitude and latitude markers assist interpretation. This approach provides an accurate and clear depiction of the modelled CRs flux distributions

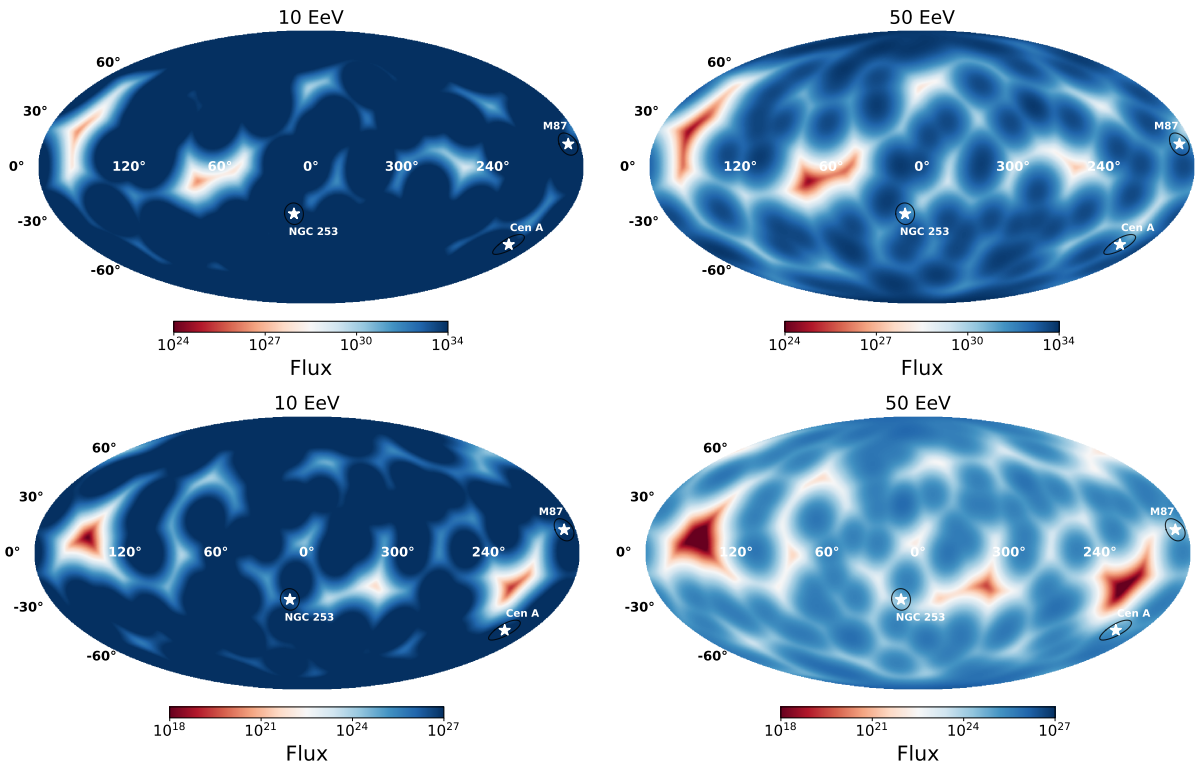


FIG. 2. UHECR flux skymaps from FSRQs (top panel) and BL Lac objects (bottom panel) for 10 EeV and 50 EeV energies.

across the sky.

The skymaps in Fig. 2 illustrate the CRs flux distributions for uniform source distribution models of the considered astrophysical sources across HEALPix pixels, with random sampling of (RA, Dec) coordinates converted into HEALPix (θ, ϕ) angles. Fig. 2 presents the full-sky distribution of UHECRs flux in Mollweide projection for two distinct classes of AGN sources, namely FSRQs and BL Lacertae (BL Lac) objects, at energies of 10 EeV and 50 EeV. The top panels correspond to the FSRQ case, while the bottom panels illustrate the BL Lac scenario. In each case, the flux intensity is represented on a logarithmic color scale, where the red regions denote comparatively lower flux values and the blue regions indicate higher flux intensities. The maps reveal distinct anisotropy patterns in the UHECRs flux distribution, particularly evident in the FSRQ case. At lower energies (10 EeV), the flux appears more diffuse, indicating a larger propagation horizon and contributions from a greater number of distant sources. However, at higher energies (50 EeV), the anisotropy becomes more pronounced, with localized enhancements of flux (blue regions) corresponding to the dominance of nearby, high-luminosity FSRQs. This behaviour arises from the increased energy losses during propagation, which restrict the contribution of distant sources and amplifies the directional dependence of the flux. In contrast, the BL Lac sources display a relatively smoother flux distribution at both energies, suggesting a weaker degree of anisotropy.

This can be attributed to their lower intrinsic luminosity and more uniform spatial distribution, which leads to a more isotropic flux pattern. Overall, the comparison between FSRQ and BL Lac source classes highlights the dependence of UHECRs anisotropy on both the source type and the cosmic ray energy, emphasizing the combined effects of source luminosity function, spatial evolution, and propagation constraints in shaping the observed flux distribution.

To identify galaxies or AGNs in the vicinity of the detected hotspots, we performed a positional cross-matching using the `astroquery.simbad` module. The coordinates of each hotspot (RA and Dec) were used as input to query the SIMBAD astronomical database within a circular search region of radius 1° . A custom SIMBAD query was configured to retrieve essential information such as the main identifier (`main_id`), object type (`otypes`), and equatorial coordinates (RA, Dec). The returned catalogue entries were then filtered to include only extragalactic sources, specifically those classified as galaxies or active nuclei. The following SIMBAD object types were considered: `G` (Galaxy), `AGN`, `Radio` (Radio Source), `Sy` (Seyfert Galaxy), and `LINER` (Low-Ionization Nuclear Emission-line Region). For each candidate object, the angular separation from the hotspot position was calculated using the `astropy.coordinates.SkyCoord` module, and only those lying within 1° were considered. This method ensures the identification of nearby galaxies or AGN-like

TABLE II. Nearby galaxies and extragalactic sources within 1° of the hotspot located at (RA = 163.42° , Dec = -88.26°) for FSRQ case.

Object Name	Type	Redshift (z)	Separation ($^\circ$)	RA ($^\circ$)	Dec ($^\circ$)
HD 89592	RG*	2.20×10^{-5}	0.503	146.63	-88.36
HD 99357	RG*	9.69×10^{-5}	0.703	166.62	-88.96
ESO 1-5	G/AG?	0.016732	0.963	133.27	-88.09
TYC 9518-226-1	RG*	1.11×10^{-4}	0.887	147.23	-89.07
CPD-87 168	RG*	5.15×10^{-5}	0.218	156.42	-88.22
CPD-87 200	RG*	1.10×10^{-4}	0.832	189.49	-88.11
CPD-87 210	RG*	8.04×10^{-5}	0.913	194.36	-88.33
TYC 9514-269-1	RG*	1.65×10^{-5}	0.860	147.88	-87.60
TYC 9514-397-1	RG*	1.37×10^{-5}	0.508	148.30	-88.09
TYC 9515-655-1	RG*	4.03×10^{-5}	0.225	164.50	-88.04
TYC 9515-917-1	RG*	8.66×10^{-5}	0.561	156.23	-87.76
TYC 9515-1068-1	RG*	2.28×10^{-5}	0.854	156.11	-87.45
TYC 9515-1109-1	RG*	1.05×10^{-4}	0.859	163.49	-87.40
TYC 9516-329-1	RG*	2.04×10^{-5}	0.891	184.90	-87.76
TYC 9516-1710-1	RG*	7.72×10^{-5}	0.687	184.11	-88.06
TYC 9518-181-1	RG*	1.18×10^{-4}	0.963	130.54	-88.72
TYC 9519-330-1	RG*	1.76×10^{-5}	0.517	171.06	-88.74
UCAC4 014-002450	RG*	1.45×10^{-4}	0.916	156.23	-87.38
UCAC4 013-002324	RG*	2.20×10^{-4}	0.904	155.85	-87.40
UCAC4 011-002319	RG*	1.38×10^{-4}	0.461	173.47	-87.94

TABLE III. Nearby galaxies and extragalactic sources within 1° of hotspot located at (RA = 235.59° , Dec = -88.45°) for BL Lac case.

Object Name	Type	Redshift (z)	Separation ($^\circ$)	RA ($^\circ$)	Dec ($^\circ$)
ESO 1-6	G	0.007538	0.909	216.83	-87.77
ESO 1-7	G	0.016581	0.650	255.69	-88.92
2MASX J15433127-8740427	G	0.04313	0.771	235.88	-87.68
NOGG P1 815	GrG	0.006525	0.917	224.90	-87.61
[TSK2008] 1026	GrG	0.007574	0.898	225.41	-87.62
CPD-88 126	RG*	2.77×10^{-5}	0.551	227.16	-88.97
TYC 9534-319-1	RG*	1.04×10^{-5}	0.860	269.06	-88.61
TYC 9520-151-1	RG*	1.91×10^{-5}	0.968	200.43	-88.36
TYC 9517-1108-1	RG*	1.19×10^{-5}	0.421	233.68	-88.03
TYC 9517-1326-1	RG*	4.50×10^{-5}	0.934	218.49	-87.70
TYC 9517-1406-1	RG*	3.70×10^{-6}	0.652	224.20	-87.91
TYC 9521-317-1	RG*	2.24×10^{-5}	0.599	212.90	-88.60
TYC 9530-981-1	RG*	1.77×10^{-4}	0.568	241.42	-87.91
TYC 9530-1462-1	RG*	4.14×10^{-5}	0.925	259.49	-87.90

sources that could be potential counterparts or contributors to the observed hotspot regions in the sky. Numerous entries are classified as **RG*** (Red Giant Stars), and some are **AG?** (possible active galaxy) and **GrG** (galaxy group).

For FSRQs, using the above method, we searched for extragalactic sources within an angular radius of 1° around the hotspot located at (RA = 163.42° , Dec = -88.26°). Notable entries from **ESO 1-5**, **CPD**, **TYC**, and **UCAC** are found in this region. The presence of nearby galaxies in the vicinity of this hotspot may suggest possible associations between these extragalactic sources and the observed high-energy CRs flux enhancement in this direction. For the BL Lac objects, among the identified sources within 1° of the hotspot located at RA = 235.59° , Dec = -88.45° , several prominent extragalactic objects

were found. A few possible active galaxies (**AG?**) like **ESO 1-6** and **ESO 1-7** were identified, suggesting the presence of AGNs in the vicinity. The catalogue also includes several **RG*** from **CPD** and **TYC** catalogue. Overall, the spatial correlation indicates that the region is populated with a mix of normal and active galaxies, as well as nearby stellar contaminants. For both FSRQs and BL Lac objects, these nearby galaxies or extragalactic sources are given in Tables II and III.

V. SUMMARY AND CONCLUSION

In this work, we have investigated the flux of UHE-CRs within the standard Λ CDM cosmology, considering

both FSRQs and BL Lac objects as potential source populations. A mixed nuclear composition consisting of p, He, N, Si, and Fe was adopted to model the CRs spectra and the corresponding shower observables $\langle X_{\max} \rangle$ and $\sigma(X_{\max})$. The theoretical predictions show a good level of agreement with the combined Auger and TA data, yielding reduced χ^2 values of 2.02 and 2.43 for the FSRQ and BL Lac scenarios, respectively. The deviation from a purely protonic composition indicates that a mixed composition provides a more realistic description of UHECRs propagation and air-shower behaviour. We find different inter-separation source distance for fitting the observable flux data at 160 kpc and 0.2 Mpc for FSRQ and BL Lac objects respectively.

The full-sky flux distributions constructed using the HEALPix formalism reveal distinct anisotropy patterns across different energy scales and source classes. In the FSRQ case, anisotropy becomes increasingly pronounced at higher energies (50 EeV), highlighting the dominance of nearby high-luminosity sources and reduced contribution from distant ones due to energy loss effects. Conversely, BL Lac sources display a relatively smoother and more isotropic flux pattern, consistent with their lower luminosity and uniform spatial distribution. These results emphasize the combined influence of source proper-

ties, spatial evolution, and propagation effects in shaping the observed UHECRs flux.

The positional cross-matching of identified hotspot regions with the SIMBAD database further supports a possible association between localized flux enhancements and nearby extragalactic sources. In particular, the hotspot near (RA = 163.42°, Dec = -88.26°) coincides with several AGNs and galaxies as given in Table II and III. Such correlations indicate that these extragalactic sources could contribute to the observed high-energy flux excess.

Overall, the present analysis demonstrates that the mixed-composition models under this method can reproduce key spectral and compositional features observed in UHECRs data. The anisotropy signatures and hotspot correlations offer potential clues to the origin of UHECRs, motivating further multi-messenger and directional studies with improved statistics and higher-resolution datasets.

ACKNOWLEDGEMENT

UDG is thankful to the Inter-University Centre for Astronomy and Astrophysics (IUCAA), Pune, India for the Visiting Associateship of the institute.

-
- [1] K. Kotera and A. V. Olinto, *Ann. Rev. Astron. Astrophys.* **49**, 119 (2011), arXiv:1101.4256 [astro-ph.HE].
 - [2] L. A. Anchordoqui, *Phys. Rept.* **801**, 1 (2019), arXiv:1807.09645 [astro-ph.HE].
 - [3] G. Sigl, F. Miniati, and T. A. Ensslin, *Phys. Rev. D* **70**, 043007 (2004), arXiv:astro-ph/0401084.
 - [4] N. Globus, D. Allard, and E. Parizot, *A & A* **479**, 97 (2008), arXiv:0709.1541.
 - [5] R. Aloisio, V. Berezhinsky, and A. Gazizov, *Astropart. Phys.* **39-40**, 129 (2012), arXiv:1211.0494 [astro-ph.HE].
 - [6] A. Aab *et al.* (Pierre Auger Collaboration), *Nucl. Instrum. Meth. A* **798**, 172 (2015), arXiv:1502.01323.
 - [7] R. U. Abbasi *et al.* (Telescope Array), *Astropart. Phys.* **80**, 131 (2016), arXiv:1511.07510 [astro-ph.HE].
 - [8] D. J. Bird *et al.* (HIRES), *Astrophys. J.* **441**, 144 (1995), arXiv:astro-ph/9410067.
 - [9] R. U. Abbasi *et al.* (Telescope Array), *Science* **382**, abo5095 (2023), arXiv:2311.14231.
 - [10] K. Greisen, *Phys. Rev. Lett.* **16**, 748 (1966).
 - [11] G. T. Zatsepin and V. A. Kuz'min, *JETP Lett.* **4**, 78 (1966).
 - [12] C. D. Dermer, S. Razzaque, J. D. Finke, and A. Atoyan, *New J. Phys.* **11**, 065016 (2009), arXiv:0811.1160 [astro-ph].
 - [13] R. U. Abbasi *et al.* (HiRes), *Phys. Rev. Lett.* **104**, 161101 (2010), arXiv:0910.4184 [astro-ph.HE].
 - [14] B. T. Zhang, K. Murase, N. Ekanger, M. Bhattacharya, and S. Horiuchi, (2024), arXiv:2405.17409 [astro-ph.HE].
 - [15] G. R. Farrar, *Phys. Rev. Lett.* **134**, 081003 (2025), arXiv:2405.12004 [astro-ph.HE].
 - [16] K. Murase, Y. Narita, and W. Yin, (2025), arXiv:2504.15272 [hep-ph].
 - [17] M. Unger and G. R. Farrar, *Astrophys. J. Lett.* **962**, L5 (2024), arXiv:2312.13273 [astro-ph.HE].
 - [18] S. P. Sarmah, P. Sarmah, and U. D. Goswami, *JHEAP* **49**, 100451 (2026), arXiv:2504.11712 [astro-ph.HE].
 - [19] S. P. Sarmah and U. D. Goswami, *Astropart. Phys.* **172**, 103138 (2025), arXiv:2411.00366 [astro-ph.HE].
 - [20] P. Abreu *et al.* (Pierre Auger Collaboration), *JCAP* **01**, 023, 2112.06773.
 - [21] R. G. Lang, *JCAP* **11**, 023, arXiv:2405.03528 [astro-ph.HE].
 - [22] D. J. Birds *et al.* (HiRes collaboration), *Phys. Rev. Lett.* **71**, 3401 (1993), arXiv:1507.06585.
 - [23] R. U. Abbasi *et al.* (HiRes collaboration), *Phys. Rev. Lett.* **100**, 101101 (2008), arXiv:astro-ph/0703099.
 - [24] J. Abraham *et al.* (Pierre Auger Collaboration), *Phys. Lett. B* **685**, 239 (2010), arXiv:1002.1975.
 - [25] J. Abraham *et al.* (Pierre Auger Collaboration), *Phys. Rev. Lett.* **101**, 061101 (2008), arXiv:0806.4302.
 - [26] P. Abreu *et al.* (Pierre Auger collaboration), *Eur. Phys. J. C* **81**, 966 (2021), arXiv:2109.13400.
 - [27] V. Verzi, D. Ivanov, and Y. Tsunesada, *PTEP* **2017**, 12A103 (2017), arXiv:1705.09111 [astro-ph.HE].
 - [28] R. Aloisio, V. Berezhinsky, and P. Blasi, *JCAP* **10**, 020, arXiv:1312.7459.
 - [29] A. Aab *et al.* (Pierre Auger Collaboration), *JCAP* **04**, 038, arXiv:1612.07155.
 - [30] A. A. Halim *et al.* (Pierre Auger Collaboration), *JCAP* **05**, 024, arXiv:2211.02857 [astro-ph.HE].

- [31] *Astrophys. J.* **743**, 171 (2011), arXiv:1108.1420 [astro-ph.HE].
- [32] M. Ajello *et al.*, *Astrophys. J.* **689**, 666 (2008), arXiv:0808.3377 [astro-ph].
- [33] Y. Inoue and T. Totani, *Astrophys. J.* **702**, 523 (2009), [Erratum: *Astrophys. J.* 728, 73 (2011)], arXiv:0810.3580 [astro-ph].
- [34] J. S. Dunlop and J. A. Peacock, *MNRAS* **247**, 19 (1990).
- [35] J. V. Wall, C. A. Jackson, P. A. Shaver, I. M. Hook, and K. I. Kellermann, *Astron. Astrophys.* **434**, 133 (2005), arXiv:astro-ph/0408122.
- [36] P. Giommi and P. Padovani, *MNRAS* **268**, L51 (1994).
- [37] T. A. Rector, J. T. Stocke, E. S. Perlman, S. L. Morris, and I. M. Gioia, *Astron. J.* **120**, 1626 (2000), arXiv:astro-ph/0006215.
- [38] A. Wolter and A. Celotti, *Astron. Astrophys.* **371**, 527 (2001), arXiv:astro-ph/0103394.
- [39] A. Caccianiga, T. Maccacaro, A. Wolter, R. Della Ceca, and I. M. Gioia, *Astrophys. J.* **566**, 181 (2002), arXiv:astro-ph/0110334.
- [40] V. Beckmann, D. Engels, N. Bade, and O. Wucknitz, *Astron. Astrophys.* **401**, 927 (2003), arXiv:astro-ph/0302242.
- [41] P. Padovani, P. Giommi, H. Landt, and E. S. Perlman, *Astrophys. J.* **662**, 182 (2007), arXiv:astro-ph/0702740.
- [42] M. Ajello, P. Rebusco, N. Cappelluti, O. Reimer, H. Boehringer, J. Greiner, N. Gehrels, J. Tueller, and A. Moretti, *Astrophys. J.* **690**, 367 (2009), arXiv:0809.0006 [astro-ph].
- [43] Y. Ueda, M. Akiyama, K. Ohta, and T. Miyaji, *Astrophys. J.* **598**, 886 (2003), arXiv:astro-ph/0308140.
- [44] G. Hasinger, T. Miyaji, and M. Schmidt, *Astron. Astrophys.* **441**, 417 (2005), arXiv:astro-ph/0506118.
- [45] F. La Franca *et al.*, *Astrophys. J.* **635**, 864 (2005), arXiv:astro-ph/0509081.
- [46] R. D. Blandford and R. L. Znajek, *MNRAS* **179**, 433 (1977).
- [47] C. M. Urry and P. Padovani, *Publ. Astron. Soc. Pac.* **107**, 803 (1995), arXiv:astro-ph/9506063.
- [48] M. J. M. Marcha, I. W. A. Browne, C. D. Impey, and P. S. Smith, *MNRAS* **281**, 425 (1996).
- [49] P. Giommi, P. Padovani, and G. Polenta, *MNRAS* **431**, 1914 (2013), arXiv:1302.4331 [astro-ph.HE].
- [50] M. Ajello *et al.*, *Astrophys. J.* **751**, 108 (2012), arXiv:1110.3787 [astro-ph.CO].
- [51] M. Ajello *et al.*, *Astrophys. J.* **780**, 73 (2014), arXiv:1310.0006 [astro-ph.CO].
- [52] G. Ghisellini, L. Maraschi, and F. Tavecchio, *Mon. Not. Roy. Astron. Soc.* **396**, 105 (2009), arXiv:0903.2043 [astro-ph.CO].
- [53] E. T. Meyer, G. Fossati, M. Georganopoulos, and M. L. Lister, *Astrophys. J. Lett.* **752**, L4 (2012), arXiv:1203.4991 [astro-ph.HE].
- [54] J. L. Han, *Annu. Rev. Astron.* **255**, 111 (2017).
- [55] Y. Hu and others., *Astrophys. J.* **941**, 133 (2022).
- [56] U. Chadayammuri, *MNRAS* **512**, 2 (2022), arXiv:2202.13430.
- [57] A. Neronov and I. Vovk, *Science* **328**, 73 (2010), arXiv:1006.3504.
- [58] L. Feretti *et al.*, *Astron. Astrophys. Rev.* **20**, 54 (2012), arXiv:1205.1919.
- [59] J. P. Vallée, *New Astro. Rev.* **55**, 91 (2011).
- [60] F. Vazza *et al.*, *Class. Quantum Grav.* **34**, 234001 (2017), arXiv:1711.02669.
- [61] D. Harari, S. Mollerach, and E. Roulet, *Phys. Rev. D* **89**, 123001 (2014), arXiv:1312.1366.
- [62] V. Berezhinsky and A. Z. Gazizov, *Astrophys. J.* **643**, 8 (2006), arXiv:astro-ph/0512090.
- [63] S. I. Syrovatskii, *Soviet Astro.* **3**, 22 (1959).
- [64] N. Aghanim *et al.* (Planck Collaboration), *A&A* **641**, A6 (2020), arXiv:1807.06209.
- [65] S. Mollerach and E. Roulet, *Phys. Rev. D* **99**, 103010 (2019), arXiv:1903.05722.
- [66] P. Blasi and A. V. Olinto, *Phys. Rev. D* **59**, 023001 (1999), arXiv:astro-ph/9806264.
- [67] S. P. Sarmah, *J. Phys. Conf. Ser.* **2957**, 012002 (2025), arXiv:2504.18987 [astro-ph.HE].
- [68] N. Globus, D. Allard, and E. Parizot, *Phys. Rev. D* **92**, 021302 (2015), arXiv:1505.01377.
- [69] T. S. *et al.*, *Phys. Rev. D* **62**, 093005 (2000), arXiv:astro-ph/0003484.
- [70] K. Kotera and M. Lemoine, *Phys. Rev. D* **77**, 123003 (2008), arXiv:0801.1450.
- [71] S. P. Sarmah and U. D. Goswami, *IJMP A* **40**, 2550085 (2024), arXiv:2412.17494.
- [72] H. Yoshiguchi, S. Nagataki, S. Tsubaki, and K. Sato, *Astrophys. J.* **586**, 1211 (2003), arXiv:astro-ph/0210132.
- [73] M. Lemoine, *Phys. Rev. D* **71**, 083007 (2005), arXiv:astro-ph/0411173.
- [74] D. Hooper, S. Sarkar, and A. M. Taylor, *Astropart. Phys.* **27**, 199 (2007).
- [75] D. Hooper, S. Sarkar, and A. M. Taylor, *Phys. Rev. D* **77**, 103007 (2008), arXiv:0802.1538.
- [76] G. Sigl, *Phys. Rev. D* **75**, 103001 (2007), arXiv:astro-ph/0703403.
- [77] R. Aloisio, *Prog. Theor. Exp. Phys.* **2017**, 12A102 (2017), 1707.08471.
- [78] S. P. Sarmah and U. D. Goswami, *Eur. Phys. J. C* **84**, 419 (2024), arXiv:2303.16678.
- [79] V. Berezhinsky and A. Z. Gazizov, *Astrophys. J.* **669**, 684 (2007), arXiv:astro-ph/0702102.
- [80] J. M. González, S. Mollerach, and E. Roulet, *Phys. Rev. D* **104**, 063005 (2021), arXiv:2105.08138.
- [81] S. Mollerach and E. Roulet, *JCAP* **10**, 013, arXiv:1305.6519v1.
- [82] S. P. Sarmah and U. D. Goswami, *Astropart. Phys.* **163**, 103005 (2024), arXiv:2309.14361.
- [83] S. P. Sarmah and U. D. Goswami, *Nucl. Phys. B* **1013**, 116851 (2025), arXiv:2406.11902.
- [84] R. Aloisio and V. Berezhinsky, *Astrophys. J.* **612**, 900 (2004), arXiv:astro-ph/0403095.
- [85] S. P. Sarmah and U. D. Goswami, *J. Subatomic Part. Cosmol.* **3**, 100072 (2025).
- [86] J. Abraham *et al.* (Pierre Auger collaboration), *Phys. Rev. Lett.* **104**, 091101 (2010), arXiv:1002.0699.
- [87] T. K. Gaisser, *Cambridge University Press* (1990).
- [88] T. K. Gaisser, R. Engel, and E. Resconi, *Cambridge University Press* (2016).
- [89] A. Aab *et al.* (Pierre Auger Collaboration), *Phys. Rev. D* **90**, 122005 (2014), arXiv:1409.4809.
- [90] R. U. Abbasi *et al.* (Telescope Array Collaboration), *Astrophys. J.* **858**, 76 (2018), arXiv:1801.09784.
- [91] K. M. Górski *et al.*, *Astrophys. J.* **622**, 759 (2005).